coatings

Article

Effect of Solidifying Structure on Centerline Segregation of S50C Steel Produced by Compact Strip Production

Kai Liu [1], Shusen Cheng [1,*], Jipeng Li [1,2] and Yongping Feng [2]

[1] School of Metallurgical and Ecological Engineering, University of Science & Technology Beijing, 30 Xueyuan Road, Haidian Dsitrict, Beijing 100083, China; beikedaliukai@163.com (K.L.); lijipeng@jiugang.com (J.L.)
[2] Jiuquan Iron & Steel (Group) Co., Ltd., Jiayuguan 735100, China; yp_0311@163.com
* Correspondence: chengsusen@metall.ustb.edu.cn

Abstract: Medium-high carbon steels having a high quality are widely used in China. It is advantageous to produce high value-added hot-rolled plates with the crystal refined and chemical composition homogenized in the casting slabs. However, element segregation occurs easily during high-medium carbon steels' production. Generally, the centerline segregation is improved by enlarging the equiaxed zone with low-superheat casting and electromagnetic stirring (EMS). Studies were conducted on centerline segregation of S50C steel slabs with a thickness of 52 mm produced by the compact strip production (CSP) process in China without EMS equipped. By sampling along the width at different position, the secondary dendrite arm spacing (SDAS) was measured after etching and picture processing, based on which the cooling rate was calculated. It was found that the cooling rate increased from the center to the surfaces of the slabs ranging in 1~20 K/s, 10 times faster than that of a conventional process. The faster cooling rate led to a refined solidifying structure and columnar dendrite through the center of the slabs. The SDAS tended to increase from surfaces to the center, ranging only 32~120 μm smaller than that of a conventional process in 100~300 μm, indicating a finer solidifying structure by the CSP process. Results by EPMA indicated that elements C, Si, and Mn distribute in dispersed spots, increasing towards the center, and the centerline segregation changed in a narrow range: for C mainly in 1.0~1.1, Si in 0.98~1.08, Mn in 0.96~1.02, respectively, meaning a more chemical homogenization than that of thick slabs. Elements' segregation originated from solute redistribution between solid and liquid. According to thermodynamic calculation, δ region of S50C is so narrow that the solute redistribution mainly occurred between γ-Fe and liquid during solidification. As the equilibrium partition coefficient of element C was the smallest, it was easy for C to be rejected to the residual liquid in the inter-dendritic space, leading to obvious segregation, relatively. Besides, as a result of high-cooling intensity, the solidifying structure became so fine that the Fourier number increased and the volume of the residual liquid decreased, making centerline segregation alleviated effectively both in volume and degree. Although bulging was observed during the industrial experiment, the centerline segregation was still inhibited obviously as the refining solidifying structure with permeability ranged only in 0.1~2.3 μm^2 from the surfaces to centerline, which showed a good resistance on the residual flow towards the centerline.

Keywords: CSP process; S50C steel; solidifying structure; cooling rate; micro-segregation; centerline segregation

check for updates

Citation: Liu, K.; Cheng, S.; Li, J.; Feng, Y. Effect of Solidifying Structure on Centerline Segregation of S50C Steel Produced by Compact Strip Production. *Coatings* **2021**, *11*, 1497. https://doi.org/10.3390/coatings11121497

Academic Editor: Awais Ahmad

Received: 6 November 2021
Accepted: 29 November 2021
Published: 5 December 2021

1. Introduction

In medium-high carbon steels' production, elements' segregation can occur easily as the solidifying range is relatively wide; thus, it has called more attention to be improved [1–3]. Usually, the micro-segregation can be reduced in the subsequent processing; however, macro-segregation [4–9], which may cause inconsistent transformation products, leading to failure of the finished products in service [10–14], is more harmful. Therefore, it is vital to control the macro-segregation at a desired level.

Actually, the segregation originates from redistribution of solutes during solidification in the solidifying front, leading to solute-enriched liquid in the inter-dendritic space, and then the liquid is driven, by some factors such as thermal shrinkage and bulging, to the centerline of slabs, forming centerline segregation finally. Therefore, the redistribution of solutes [15], solidifying structure, and the motion of the solute-enriched liquid in the inter-dendritic space would have an important effect on the centerline segregation; commonly, the element segregation degree is used to describe the extent of the element segregation, shown as follows [16]:

$$r_i = C_i / C_{i0} \quad (1)$$

where C_i is the concentration of solute i at a certain position of the slabs, and C_{i0} is the nominal concentration of solute i.

Currently, many actions have been taken to improve the internal quality of casting billets, such as electromagnetic stirring (EMS) [17–23], soft reduction, etc. Most of the actions taken are to enlarge the equiaxed zone and dismiss the shrinkage so that the segregation could be inhibited effectively [24–27]. Ma and Zhang et al. [28] simulated the center macroscopic segregation process of Q345 slabs, producing in a conventional process at a casting speed of 0.85 m/min with mechanical reduction, and the results showed that the segregation could be improved by an amount of 10 mm of reduction at the position with 0.4 of liquid fraction, which was verified by experiments, indicating that the segregation degree of C ranged from 0.7~1.2. However, in addition to the cost of such expensive equipment, it is always difficult to determine the reasonable position and operative parameters for the equipment, as the complexity of the industrial plants and the solidifying characteristics of a certain steel grade [29]. Additionally, according to Tsuchida and O. Haida [30,31], few effects have EMS and soft reduction on the volume of solute-enriched liquid transported to the centerline of the slabs to form the centerline segregation: EMS may improve the degree of segregation but enlarges the zone of segregation, and, though the thickness of segregation might be minimized by soft reduction, the degree of segregation becomes heavier.

With a higher cooling intensity, faster heat transfer, and thinner dimension, it is advantageous for the CSP process to improve the internal quality of slabs. The CSP process, as shown in Figure 1, is characterized by high cooling rate, compact layout, and lower energy consumption, making the casting speed rise to 4.0~6.0 m/min, and has been thriving for decades [32–34].

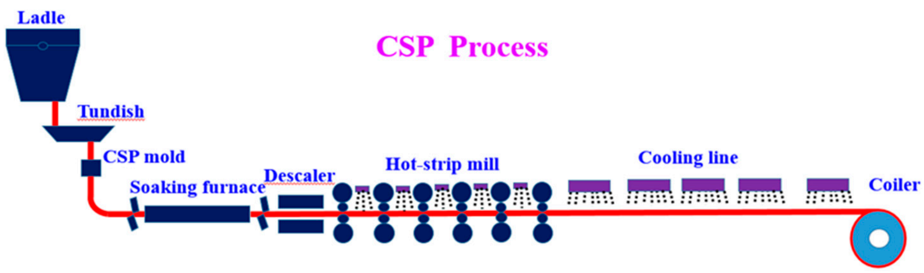

Figure 1. Schematic representation of CSP plant.

Connected with a rolled-hearth tunnel furnace from the caster to the hot rolling mill, in a CSP process the slabs, unlike the conventional process, have experienced only $L \rightarrow L + \delta\text{-Fe} \rightarrow L + \gamma\text{-Fe} \rightarrow \gamma\text{-Fe}$ before finishing rolling. As shown in Figure 2, $R(1)$ represents the solidification sequence of the CSP process and $R(2)$ and $R(3)$ represent the solidification sequence of conventional casting ($R(2)$ is reheated from 600 °C while $R(3)$ is from room temperature), respectively. From Figure 2, $R(1)$ indicates that the liquid steel solidifies with a relatively higher cooling rate and the surface temperature of the slab is above A_3 at about 1000 °C before entering the soaking furnace. Then, the slab is directly transported into the soaking furnace, preparing for finishing rolling. While both $R(2)$ and $R(3)$ solidify with lower cooling rates and were cooling down below A_1, and reheated over A_3 before rolling.

Consequently, solidifying structure of slabs produced by CSP is finer, resulting in inhibiting elements' segregation. Additionally, slabs produced by CSP remain above A_3, avoiding precipitation before rolling, which is of great advantage for chemical homogenization, such that the strips exhibit a greater uniformity as regards chemical composition, microstructure, mechanical properties, and dimensional accuracy [35,36].

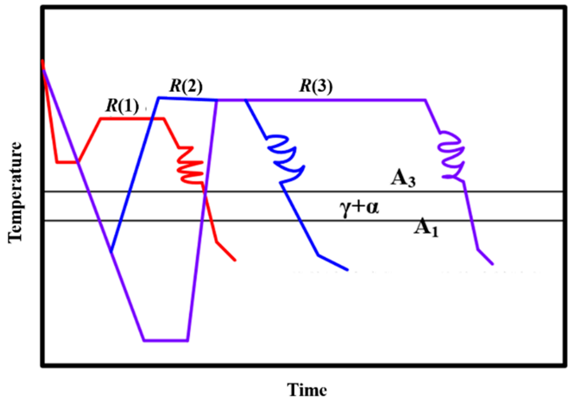

Figure 2. Comparison between conventional casting and compact strip processing.

However, for now, there is little literature, especially for producing medium-high carbon steels, reporting the solidifying structure, element segregation, and the mechanism for the formation of centerline segregation during a CSP process sufficiently and systematically. In view of this, the objective of present work was to investigate the solidifying structure, element segregation, and the improvement of element segregation with the solidifying structure refined for S50C steels produced by CSP process.

In this contribution, samples were collected from a CSP plant in China without electromagnetic stirring, and the studies on the solidifying structure and segregation of S50C steel were conducted systematically from micro scale to macro scale. The results of the present work will give a deep insight to a solidifying structure and the segregation for the CSP process.

2. Experimental Method

The present study mainly included several activities, as follows:

- Collection of samples from an industrial trial in a CSP plant in JISCO in Jiuquan, China.
- Measurement of SDAS by sampling from the transverse section of thin slab (with a dimension 1270 mm × 52 mm) samples.
- Micro-segregation tests for elements C, Si, and Mn by EPMA (Electron Probe Microanalysis, EPMA-1720H, Shimadzu, Kyoto, Japan) through mapping scanning mode.
- Macro-segregation tests by OES (Optical Emission Spectrometer-ARL8860, Thermo Fisher Scientific, Waltham, MA, USA).
- Calculation for macro-segregation degree for elements C, Si, and Mn.

The slab samples were collected from a CSP plant in China, together with the corresponding chemical composition, as shown in Table 1.

Table 1. Nominal Composition (mass percent, %).

C	Si	Mn	P	S
0.48	0.18	0.64	0.0082	0.0021

The CSP process is characterized by a high casting speed and high cooling rate, and the primitive process parameters are listed in Table 2 for the present work.

Table 2. The primitive process parameters in the present work.

Parameters	Value
Casting speed/m·min^{-1}	4.5
Superheat degree (K)	33
Specific water flow of second cooling zone (L·kg^{-1})	2.8
Liquidus temperature (K)	1763

After getting samples from the plant, one of the slabs was cut into a smaller size with a limited dimension, as shown in Figure 3a, where the label number started from the narrow side with 1 and ended with 9 at the center of the slab width. To reveal the details of SDAS, samples were fine-ground and polished so that a smooth surface was obtained. Then, the samples were etched with picric acid for 10 min at 70 °C. After being etched, the samples were cleaned by alcohol. Then, the morphology of the dendrite arms was observed through the whole sample surface (with an area about 4 mm × 4 mm) with LEXT OLS4100 Laser Scanning Confocal Microscope (Olympus Corporation, Tokyo, Japan). Finally, the image analyzer, Image Pro Plus 6.0, was employed to measure the SDAS, as shown in Figure 3b, and at least 30~50 measurements were taken for each zone. The data of the SDAS can be used for the calculation of the cooling rate ε during solidification, by Equation (2):

$$\lambda_s = \alpha\varepsilon^{-n} \tag{2}$$

where λ_s is SDAS in μm, ε is the cooling rate in K·s^{-1}, and α and n are constants. According to Jacobi and Schwerdtfeger [16], the value of α is 109.2 and n is 0.44; so, Equation (2) can be expressed as:

$$\lambda_s = 109.2\varepsilon^{-0.44} \tag{3}$$

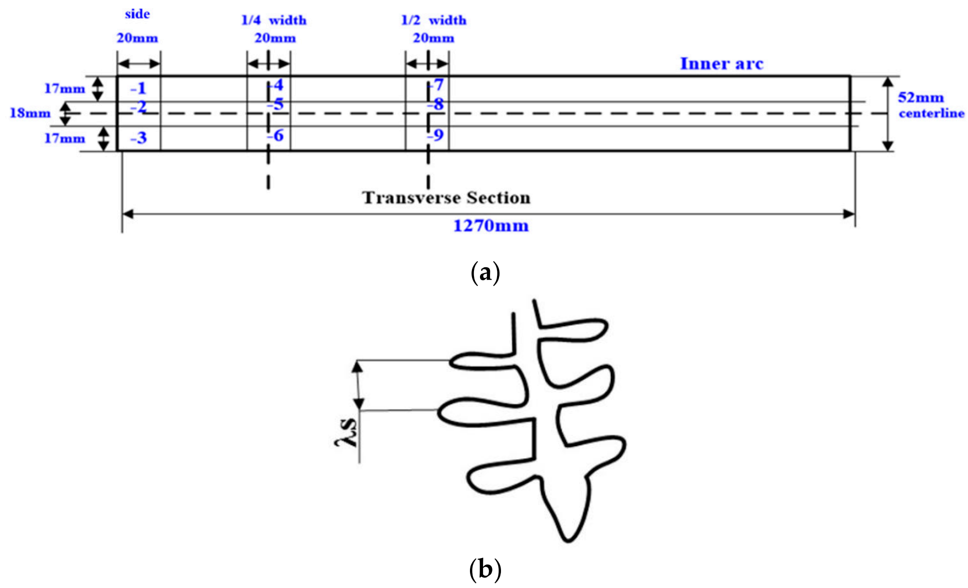

Figure 3. Sampling and measurement: (**a**) sampling for SDAS and EPMA; (**b**) measurement of SDAS.

Sampling for EPMA tests is also shown in Figure 3a. The samples were ground and polished to get a smooth surface, and the mapping scanning mode, set with a working distance of about 11 mm, an accelerating voltage of 15 kV, and a beam current of 15 nA, was used to obtain the distribution of elements C, Mn, and Si.

As shown in Figure 4, the macro-segregation was measured every 5-mm interval by OES, represented by the circles on the transverse section, and the calculation for the segregation degree of each measured element is given, as Equation (1).

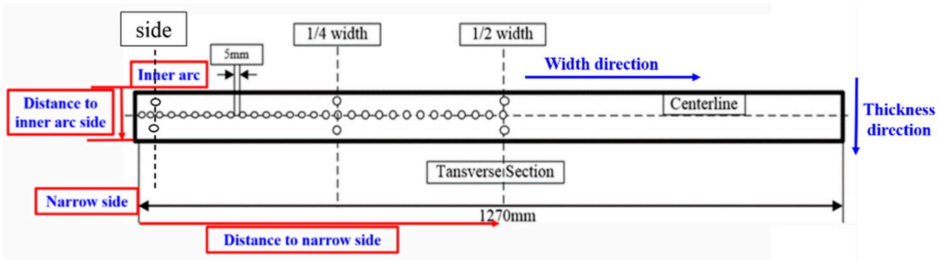

Figure 4. Testing position for OES.

3. Results and Discussion

3.1. Morphology of Solidifying Structure

Figure 5 shows the morphology of the solidifying structure produced by the CSP process. As shown in Figure 5, the solidifying structure consisted of a chill zone a few millimeters beneath the surface (Figure 5a,c) and a coarsened columnar dendrites' zone after the chill zone towards the center of the studied slabs (Figure 5b). It is obvious that, unlike attempting to enlarge the equiaxed zone during a conventional continuous cast process [17–23], the centerline of slabs produced by the CSP process was occupied by columnar dendrites (Figure 5b). The fine chill zone reflected the solidification with a rapid cooling rate in the meniscus, beyond which the columnar dendrites became coarsened towards the center of the slab. The orientation of the columnar dendrites illustrated that the direction of heat extraction was almost vertical to the surface of the slab; in other words, the solidification that occurred in the CSP process can be treated as one-dimension heat extraction.

The SDAS (λs) was measured from both surfaces towards the center of the slab, as shown in Figure 6. As can be seen from Figure 6, the SDAS tended to increase towards the center of the slabs, and the values of λs ranged from 32~120 μm, while λs of the thick slab (235 mm thick) varied over a wider range, from 100~300 μm, with bigger values [10,37]. Therefore, the solidifying structure produced by CSP was finer than that in a conventional thick slab process.

3.2. Micro-Segregation

The distribution of elements in micro scale was measured by EPMA using the mapping scanning mode, and the results are shown in Figure 7.

Figure 7 depicts the distribution of elements C, Si, and Mn in the inter-dendritic space in a microscopic scale. As can be seen, the micro-segregation distributed as dispersed spots, indicating a relatively homogeneous distribution of elements. This is because the size of the inter-dendritic space was small, resulting in the decreasing of the volume of residual liquid in it. But the micro-segregation tended to become serious from the surface to the center of the slabs, as the same trend of SDAS, among which the distribution of C was far more non-uniform compared with Si and Mn. This is because the value of partition coefficient of C (k_c) was smaller than that of Mn (k_{Mn}) and Si (k_{Si}) [15], indicating that there would be more element C in the residual liquid, which will be discussed later.

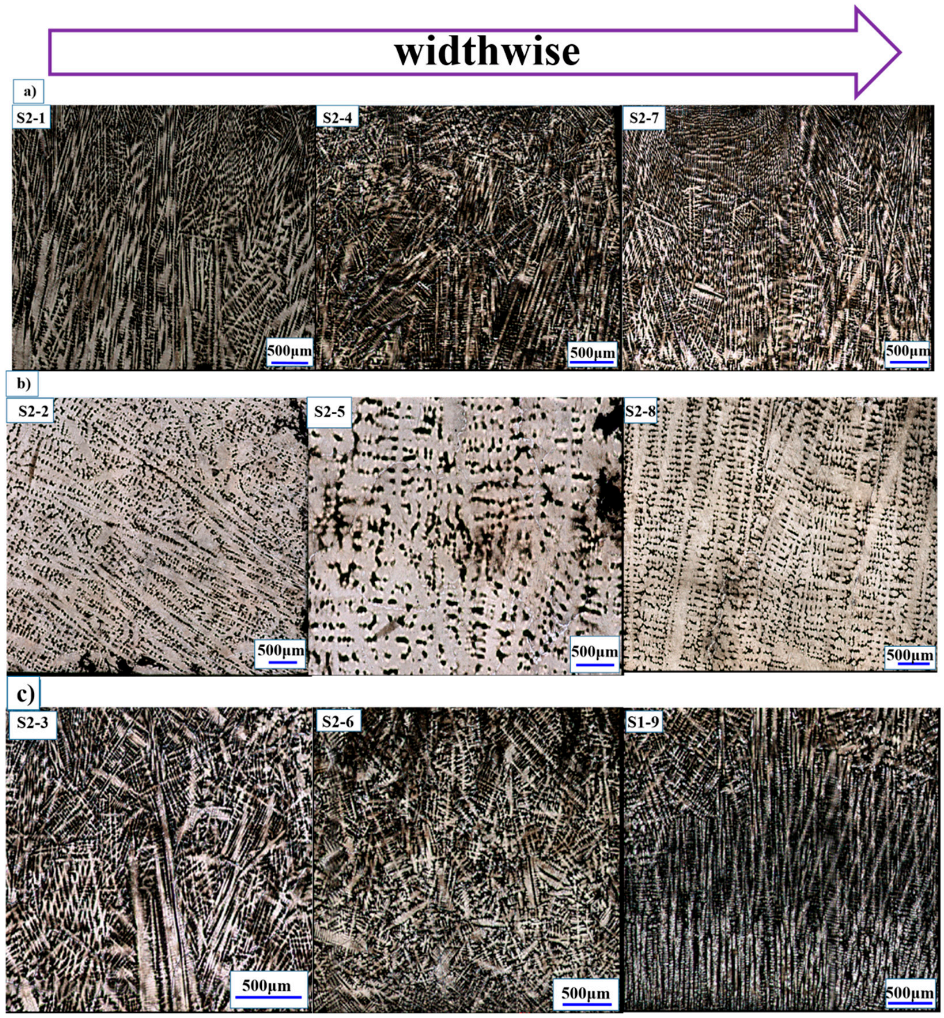

Figure 5. Morphology of Solidifying Structure by CSP: (**a**) near inner arc; (**b**) around centerline; (**c**) near outer arc.

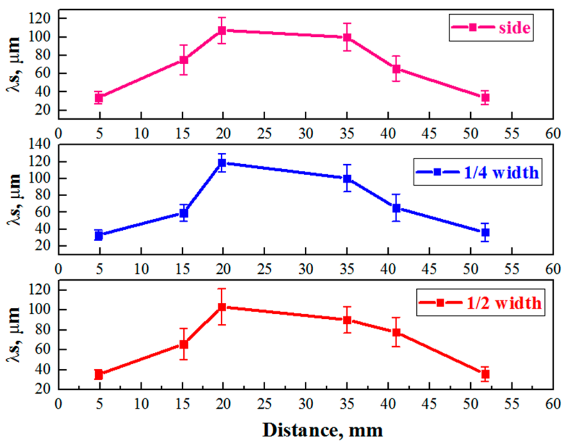

Figure 6. SDAS from surface to the center of slabs.

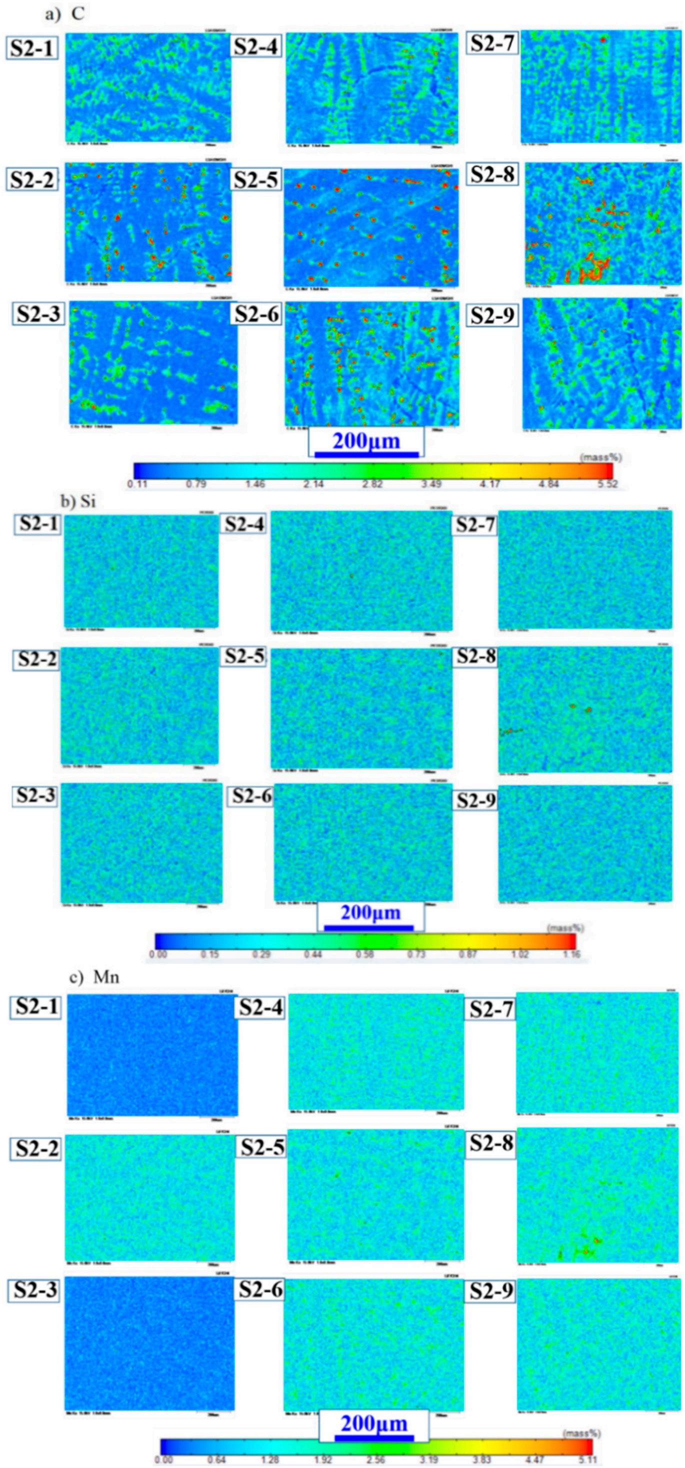

Figure 7. Results of EPMA: (**a**) C (**b**) Si (**c**) Mn.

3.3. Centerline Segregation

The centerline segregation is shown in Figure 8, in which the x-axis represents the distance to the narrow side along the centerline of the slabs' transverse section, schematically shown in Figure 4, and the y-axis indicates the extent of the element segregation calculated by Equation (1). Besides a few scattered points around 1.1, r_C was mainly in the range of 1.0 to 1.1, which shows the trend to increase towards the half width, while the segregation degree for Si and Mn was so small that the value of the segregation degree only varied mainly in the range of 0.98 to 1.08 and 0.96 to 1.02, respectively [28].

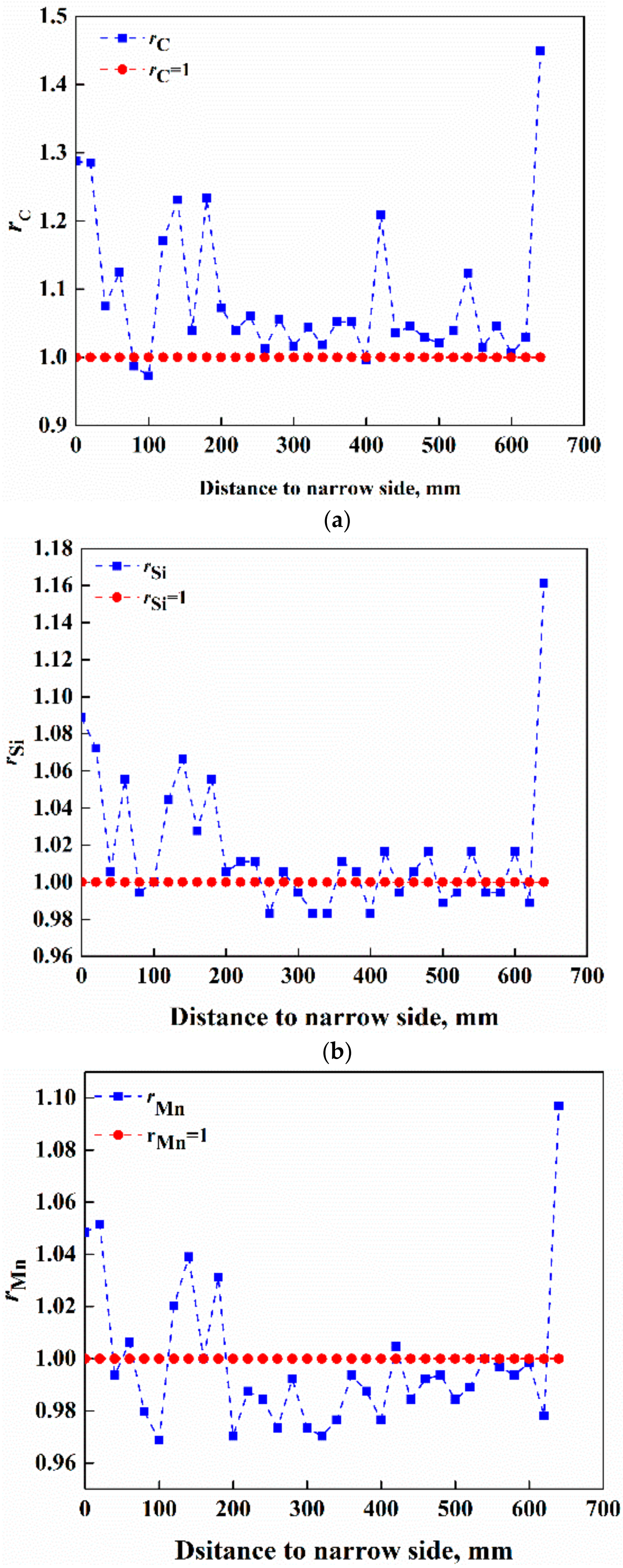

(**a**)

(**b**)

(**c**)

Figure 8. Centerline segregation degree (**a**) $r_{C,}$ (**b**) r_{Si}, and (**c**) r_{Mn}.

Figure 9 illustrates the segregation along the thickness of the slabs. As shown in Figure 9, the segregation tended to be more serious towards the center of the slabs, but the value of each element was very small, especially for elements Si and Mn, both of which ranged very little around 1.0. The centerline segregation was relatively obvious for element C, and the values of element C segregation ranged from 1.0~1.1 at both one-quarter and one-half width of the slabs, meaning that the macro-segregation of S50C steel produced by the CSP process was homogeneous along the thickness.

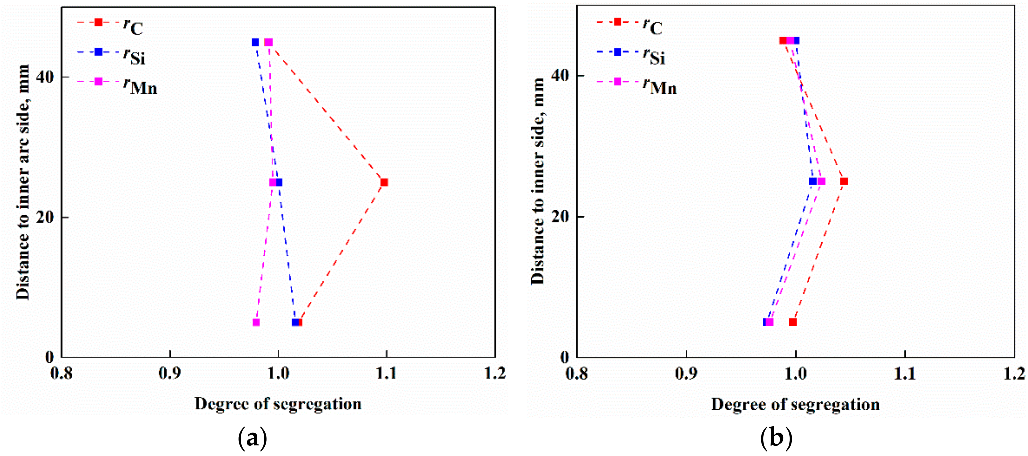

Figure 9. Macro-segregation along thickness direction: (**a**) one-quarter width, (**b**) one-half width.

According to literature [38], the macro-segregation depends on (1) partition coefficient (k) of solute elements and the parameter, R/k_m (R growth rate and k_m mass transfer coefficient), (2) morphology of the solidifying structure, (3) movement of solid and liquid phases during solidification, and (4) the extent of chemical reactions during freezing. In the current study, the (1), (2) and (4) were treated as the same for a certain element in the same position. Considering the bulging of the slab may have an influence on the movement of solid and liquid phases, i.e., factor (3), the thickness along the width direction was measured and is illustrated in Figure 10, where the x-axis represents the distance to the narrow side of the slabs along (as shown in Figure 4) the centerline, and the y-axis reflects the thickness of the slabs measured at intervals of a certain distance along the width direction of the slab.

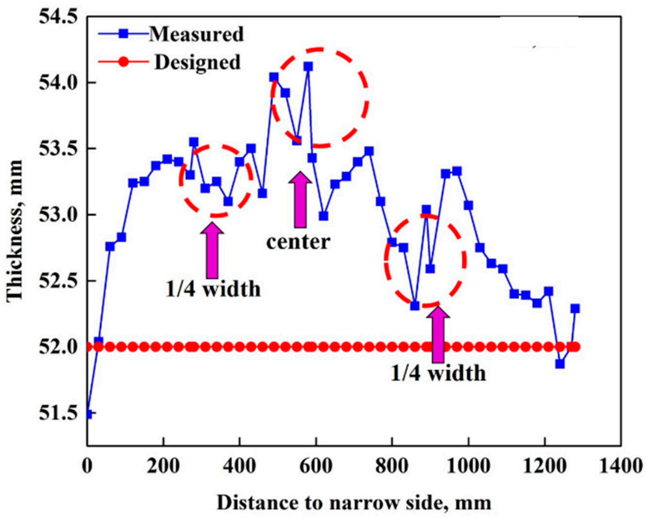

Figure 10. Thickness changes along the width direction.

As illustrated in Figure 10, the thickness of the slab increased (bulging) from both narrow sides towards the half width with the same trends of the centerline segregation degree, as shown in Figure 8. It is clear from Figure 10 that the slab, with the designed thickness of 52 mm, was about 54 mm around the center part. It is the bulging that caused the motion of the inter-dendritic liquid phase to the center of the slabs, forming the centerline segregation finally, and, because the bulging around the half width was heavier than that around the quarter width, resulting in more serious centerline segregation around the half width. Therefore, the formation of macro-segregation in the CSP process was determined mainly by bulging, which is also the key factor to control the macro-segregation during a CSP process.

3.4. Analysis on the Formation of Centerline Segregation during CSP Process

It is well known that the element segregation originates from the redistribution between the solid and liquid phases, around the solid–liquid interface. The partition coefficient determines the degree of the solutes rejected to the liquid. Usually, the partition coefficient of elements in the steel is smaller than 1.0, meaning that the solutes would be rejected from solid phase to liquid phase, forming the solute-enriched residual liquid. Then, the residual liquid remains in the inter-dendritic space. If the residual liquid solidified locally, the segregation might occur in a micro scale. In this case the degree of segregation was determined by: (1) the deviation of partition coefficient from 1.0 (the smaller the partition coefficient is, the heavier the segregation degree would be) and (2) the size of the inter-dendritic space (the finer the solidifying structure is, the smaller the amount of residual liquid remaining in the inter-dendritic space would be). Actually, the residual liquid in the inter-dendritic space may be driven to move towards a certain position (centerline) by some factors (such as bulging and thermal shrinkage) [27,39]. Then, the residual liquid converges in the very place, forming the macro-segregation (centerline segregation, as an example) finally. During this process, the motion of the residual liquid in the mushy zone plays an important role on the formation of macro-segregation [40].

According to literature [41], the cooling rate of thin slab casting and direct rolling technology is 10 times faster than that of a traditional thick slab process, resulting in a finer solidifying structure. To reveal the effects of the CSP process on the formation mechanism of S50C slabs, the main aspects, including (1) chemical composition, (2) cooling rate, and (3) the effects of solidifying structure on the flow of residual liquid, were analyzed subsequently.

(1) Chemical composition

The chemical composition (as listed in Table 1) determines the phase transformation process during solidification and the partition coefficient. By using Factsage7.0, the phase transformation process and equilibrium partition coefficient were calculated, as shown in Figures 11 and 12, respectively.

Connected with a rolled-hearth tunnel furnace from the caster to the hot rolling mill (Figure 1), the CSP process cancelled the reheating process, avoiding cooling down below $A_1 \rightarrow$ reheating to the A_3 process, so that the slabs would remain in the γ region after solidification before finishing rolling. Based on that, the results of phase transformation were calculated and are shown in Figure 11.

As shown in Figure 11, S50C steel experienced $L \rightarrow \delta \rightarrow \gamma$ transformation process before finishing rolling, and the region of δ was so narrow that it can be neglected. Therefore, within the mushy zone, the redistribution of solutes occurs mainly between γ and L, and the partition coefficient of solute i (${k_i}^{\gamma}$) between γ and L was taken to characterize the redistribution during solidification.

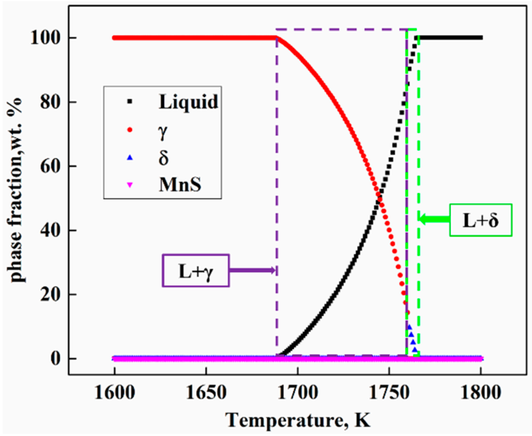

Figure 11. Phase transformation of S50C steel.

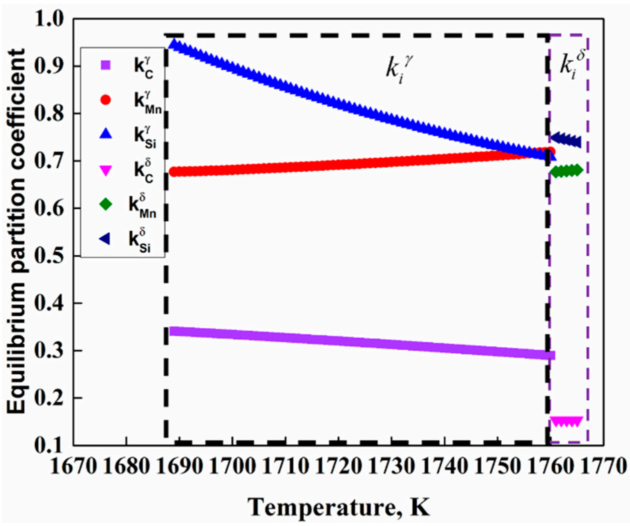

Figure 12. The equilibrium partition coefficient of S50C steel.

Figure 12 depicts the equilibrium partition coefficient of S50C during phase transformation. Both ${k_C}^\delta$ and ${k_{Mn}}^\delta$ increased to ${k_C}^\gamma$ and ${k_{Mn}}^\gamma$ around 1760 K, after which ${k_C}^\gamma$ and ${k_{Mn}}^\gamma$ changed a little with temperature, while ${k_{Si}}^\delta$ decreased to ${k_{Si}}^\gamma$ around 1760 K, then increased with temperature decreasing. Therefore, with the temperature decreasing, δ-Fe emerged firstly in the liquid, and the solutes redistributed between δ-Fe and liquid. The δ region was so narrow that γ-Fe emerged in the liquid quickly, and then the redistribution occurred between γ-Fe and liquid over a long range. Because ${k_C}^\gamma$(0.34) was the smallest, there was more element C rejected to the residual liquid, resulting in the degree of micro-segregation of C being more serious than Mn and Si, as shown in Figure 7.

(2) Cooling rate

The relationship between the cooling rate and λs is expressed in Equation (2). The results of the cooling rate (ε) for present work are shown in Figure 13, where the x-axis represents the distance to the inner arc side along the thickness direction, as shown in Figure 4, and the y-axis is the cooling rates calculated by Equation (3). As can be seen from Figure 13, the cooling rate tended to decrease to be a constant from the surface to the center zone. The values of the cooling rate varied in the range of 1 to 20 K/s.

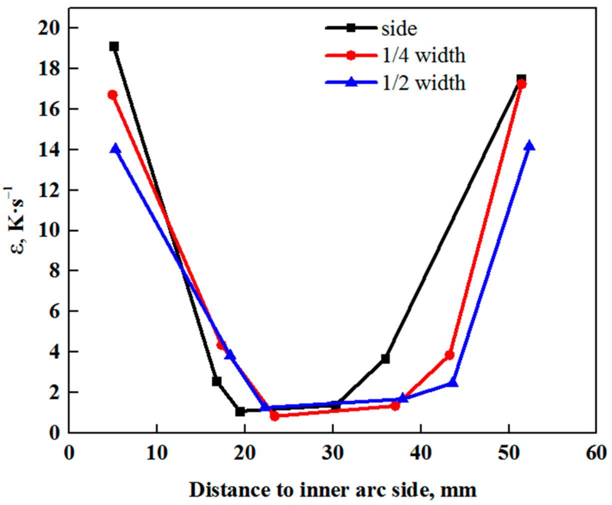

Figure 13. Results of cooling rate.

According to [42], within the mushy zone, the elements converged in the inter-dendritic space during solidification and can be described by:

$$C_L{}^* = C_0[1 - \frac{f_s}{\alpha k_0 + 1}]^{(k_0 - 1)} \tag{4}$$

where C_0 and C_L^* are the nominal concentration and concentration of solute in the liquid around the solid–liquid interface, respectively; f_s is the volume fraction of the solid phase in the mushy zone; k_0 is the partition coefficient of solute; and α is the diffusion parameter (Fourier number). Usually, $k_0 < 1$ and $f_s > 0$ during solidification; so Equation (4) indicates that the solute would decreases if α increase, and α could be written as:

$$\alpha = \frac{D_s}{\frac{\lambda_s{}^2}{4t_f}} \tag{5}$$

where D_s is the diffusivity of solute element and t_f is the local solidification time. It is obvious that Equation (5) indicates the accumulation of solutes in the inter-dendritic space within a length of $\lambda s/2$ during solidification. Therefore, with λs decreasing, the solute elements enriched in the inter-dendritic space would decrease. As shown in Figure 6, λs increased from the surface towards the center of the slab, so the solute enriched in the inter-dendritic also increased, leading to a heavier segregation degree, as shown in Figure 7.

However, it must be clarified that during the CSP process, the slabs remained in γ-Fe before finishing rolling, so that the segregation degree of element C could be improved by diffusion as the diffusivity of C was bigger [43,44], rather than the facts that the samples were taken by cooling down to the room temperature rapidly without enough time and temperature remained for elements' diffusion, which indicated that the CSP process was advantageous at inhibiting the elements' segregation.

(3) Effect of solidifying structure on the motion of liquid in mushy zone

Actually, the macro-segregation is always due to a relative velocity of the liquid of enriched solutes with respect to the solid phase, which can be induced by thermo-solute convection, forced convection, solidification shrinkage, transport and sedimentation of grains, or deformation of the solid skeleton [45,46], leading to centerline segregation in continuous casting of steel. Therefore, the factors that have a resistance on the flow can improve the centerline segregation during continuously casting slabs. Practically, the segregation originating within mushy zone consisted of dendritic arms, which can be treated as a porosity medium, and the flow in the porosity medium space can be described by D'Arcy's law, by which the velocity (v) of inter-dendritic liquid can be written as [47–49]:

$$v = -\left(\frac{K_p}{\mu g_L}\right)(\nabla P - \rho g) \quad (6)$$

where μ is the viscosity of the inter-dendritic liquid, $N \cdot s \cdot m^{-2}$; g_L is the volume fraction of the inter-dendritic liquid; P is the pressure, $N \cdot m^{-2}$; ρ is the density of the inter-dendritic liquid, $kg \cdot m^{-3}$; g is the gravitational acceleration, $m \cdot s^{-2;}$ and K_p is the specific permeability of the solid-liquid zone, m^2.

In different processes, K_p varies, which has an important influence on the flow in the inter-dendritic region. The relationship between K_P and λs is expressed as [50]:

$$K_P = \frac{\lambda_s^2 \times (1 - g_s)^3}{180 \times g_s^2} \quad (7)$$

where g_s is the fraction of solid phase, usually $g_s = 0.75$ [51,52]; so K_P can be determined by λs.

Based on the measured data, K_p was calculated by Equation (7), and the results are shown in Figure 14, in which the x-axis is the distance to the inner arc side of the slab along the thickness direction, as shown in Figure 4, and the y-axis is the value of K_P calculated by Equation (7). K_p increased from surface to the center of the slabs, just the same as λs, and it changed from 0.1~2.3 μm^2, indicating an obvious resistance of inter-dendritic flows, because of which the centerline segregation was alleviated significantly.

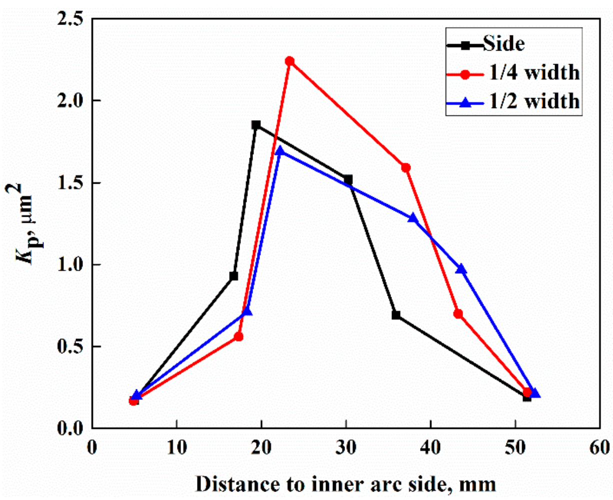

Figure 14. Results of permeability along slab thickness.

Based on what have been analyzed above, the advantages of a CSP process at alleviating segregation even without EMS are that as the cooling rate is high, as shown in Figure 13, the solidification proceeds immediately, leading to a refining of the solidifying structure, and the higher the cooling rate is, the finer the solidifying structure would be, as shown in Figure 6. Usually, the solidification of alloy is always accompanied with redistribution of solute as a result of the difference of solubility between solid and liquid, which could be characterized by equilibrium partition coefficient (k_i), as shown in Figure 12. But it is hard to solidify under equilibrium condition, which brings the assumption that the equilibrium was obtained only around the solid–liquid interface [28,42], from which the solutes were rejected to liquid phase (as $k_i < 1$), forming the solutes-enriched liquid among the inter-dendritic space, and at the same time the solutes could diffuse into the solid phase. The results of EPMA, shown in Figure 7, illustrated the elements' distribution throughout the dendrites qualitatively. Generally, the inter-dendritic liquid would be driven by thermal shrinkage and bulging (shown in Figure 10) to flow towards the centerline where centerline segregation came up. However, the flow would be resisted by a low permeability (K_P), as shown in Figure 14, so the centerline segregation was improved.

As is mentioned above, the bulging of the slabs drove the flow of the inter-dendritic liquid, but SDAS of slabs produced by CSP process was finer than that of conventional process; so, the centerline segregation was inhibited by the refining SDAS obviously, even though without EMS [17–23]. On a summary, unlike suppressing segregation by enlarging the equiaxed zone with EMS during conventional process, the CSP process is of great advantage for improving the segregation with a finer solidifying structure and higher cooling rate, even without EMS [30,31], and as the bulging had an obvious influence on the formation of centerline segregation, it needs more attention to be paid to control the bulging.

4. Conclusions

This study was mainly focused on the centerline segregation of S50C steel produced by CSP without EMS in China, and the effects of solidifying structure are analyzed on inhibition of centerline segregation. The conclusions are as follows:

(1) The cooling rate of CSP process increases from center to the surfaces of the slabs ranging from 1~20 K/s, 10 times faster than that of a conventional process. The faster cooling rate leads to refined solidifying structure and columnar dendrite through the center of the slabs. The SDAS tends to increase from surfaces to the center, ranging only from 32~120 μm, smaller than that of a conventional process, in 100~300 μm, indicating a finer solidifying structure by CSP process.

(2) According to thermodynamic calculation, δ region of S50C is so narrow that the solute redistribution mainly occurs between γ-Fe and liquid during solidification. As the equilibrium partition coefficient of element C is the smallest, it is easy for C to be rejected to the residual liquid in the inter-dendritic space leading to obvious segregation relatively.

(3) Results by EPMA indicate that elements C, Si, and Mn distribute in dispersed spots, increasing towards the center, and the centerline segregation changes in a narrow range: for C mainly in 1.0~1.1, Si in 0.98~1.08, and Mn in 0.96~1.02, respectively, meaning a more chemical homogenization than that of thick slabs.

(4) The segregation is suppressed mainly by refining the solidifying structure during CSP process. As a result of high-cooling intensity, the solidifying structure of slabs becomes so much finer that the Fourier number increases and the volume of the residual liquid decreases, making centerline segregation alleviated effectively both in volume and degree, even without EMS.

(5) Although bulging was observed during the industrial experiment, the centerline segregation was still inhibited obviously with permeability ranging only from 0.1~2.3 μm^2 from surfaces to centerline as a result of the refining solidifying structure, which showed a good resistance on the residual flow towards the centerline.

Author Contributions: Supervision, S.C.; Validation, J.L. and Y.F.; Writing—original draft, K.L. All authors have read and agreed to the published version of the manuscript.

Funding: This research was funded by National Natural Science Foundation of China No.: 62071034.

Institutional Review Board Statement: Not applicable.

Informed Consent Statement: Not applicable.

Data Availability Statement: Data is contained within the article.

Acknowledgments: The authors would like to thank National Natural Science Foundation of China No. 62071034, and the management of Jiuquan Iron & Steel (Group) Co., Ltd., China, for giving permission to publish this work.

Conflicts of Interest: The authors declare no conflict of interest.

References

1. Flemings, M.C. Our understanding of macro-segregation past and present. *ISIJ Int.* **2000**, *40*, 838–841. [CrossRef]
2. Brimacombe, J.K. The challenge of quality in continuous casting processes. *Met. Mater. Trans. A* **1999**, *30*, 553–566. [CrossRef]
3. Flemings, M.C. *Modeling of Casting, Welding and Advanced Solidification Processes-VIII*; Thomas, B.G., Beckermann, C., Eds.; TMS: Warrendale, PA, USA, 1998.
4. Cui, K.K.; Fu, T.; Zhang, Y.Y.; Wang, J.; Mao, H.B.; Tan, T.B. Microstructure and mechanical properties of $CaAl_{12}O_{19}$ rein-forced Al_2O_3-Cr_2O_3 composites. *J. Eur. Ceram. Soc.* **2021**, *41*, 7935–7945. [CrossRef]
5. Wang, J.; Zhang, Y.; Cui, K.; Fu, T.; Gao, J.; Hussain, S.; AlGarni, T.S. Pyrometallurgical recovery of zinc and valuable metals from electric arc furnace dust—A review. *J. Clean. Prod.* **2021**, *298*, 126788. [CrossRef]
6. Sung, P.K.; Poirier, D.R.; Yalamanchili, B. Segregation of carbon and manganese in continuously cast high carbon steel for wire rod. *Ironmak. Steelmak.* **1990**, *17*, 424–430.
7. Cui, K.K.; Zhang, Y.Y.; Fu, T.; Hussain, S.; Algarni, T.S.; Wang, J.; Zhang, X.; Ali, S. Effects of Cr_2O_3 content on microstructure and mechanical properties of Al_2O_3 matrix composites. *Coatings* **2021**, *11*, 234. [CrossRef]
8. Iwata, H.; Yamada, K.; Fujita, T.; Hayashi, K. Electromagnetic stirring of molten core in continuous casting of high carbon steel. *Trans. Iron Steel Inst. Jpn.* **1976**, *16*, 374–381. [CrossRef]
9. Mori, H.; Tanaka, N.; Sato, N.; Hirai, M. Macrostructure of and segregation in continuously cast carbon steel billets. *Trans. Iron Steel Inst. Jpn.* **1972**, *12*, 102–111. [CrossRef]
10. Zhou, T.; Zhang, P.; Kuuskman, K.; Cerilli, E.; Cho, S.-H.; Burella, D.; Zurob, H.S. Development of medium-to-high carbon hot-rolled steel strip on a thin slab casting direct strip production complex. *Ironmak. Steelmak.* **2017**, *45*, 603–610. [CrossRef]
11. Xiao, Y.; Li, W.; Zhao, H.; Lu, X.; Jin, X. Investigation of carbon segregation during low temperature tempering in a medium carbon steel. *Mater. Charact.* **2016**, *117*, 84–90. [CrossRef]
12. Lesoult, G. Macrosegregation in steel strands and ingots: Characterisation, formation and consequences. *Mater. Sci. Eng. A* **2005**, *413–414*, 19–29. [CrossRef]
13. Miyamura, K.; Taguchi, I.; Soga, H. New evaluation techniques of segregation in continuously cast steel. *Trans. Iron Steel Inst. Jpn.* **1984**, *24*, 883–890. [CrossRef]
14. Sirgo, J.A.; Campo, R.; Lopez, A.; Diaz, A.; Sancho, L. Measurement of centerline segregation in steel slabs. In Proceedings of the Conference Record of the 2006 IEEE Industry Applications Conference Forty-First IAS Annual Meeting, Tampa, FL, USA, 8–12 October 2006; Volume 1, pp. 516–520.
15. Ghosh, A. *Principles of Secondary Processing and Casting of Liquid Steel*; Oxford & IBH Publishing: New Delhi, India, 1990; p. 174.
16. Jacobi, H.; Schwerdtfeger, K. Dendrite morphology of steady state unidirectionally solidified steel. *Met. Mater. Trans. A* **1976**, *7*, 811–820. [CrossRef]
17. Ayata, K.; Mori, T.; Fujimoto, T. Improvement of macro-segregation in continuously cast bloom and billet by electromagnetic stirring. *Tran. Iron Steel Inst. Jpn.* **2006**, *24*, 931–939. [CrossRef]
18. Song, X.P.; Cheng, S.S.; Cheng, Z.J. Mathematical modelling of billet casting with secondary cooling zone electromagnetic stirrer. *Ironmak. Steelmak.* **2013**, *40*, 189–198. [CrossRef]
19. Trindade, L.; Vilela, A.; Filho, A.F.F.; Vilhena, M.; Soares, R. Numerical model of electromagnetic stirring for continuous casting billets. *IEEE Trans. Magn.* **2002**, *38*, 3658–3660. [CrossRef]
20. Javurek, M.; MBarna, M.; Gittler, P. Flow Modelling in round bloom strands with electromagnetical stirring. In Proceedings of the Steelsim, Graz, Austria, 1 January 2007.
21. Liu, H.; Xu, M.; Qiu, S.; Zhang, H. Numerical simulation of fluid flow in a round bloom mold with in-mold rotary electromagnetic stirring. *Met. Mater. Trans. A* **2012**, *43*, 1657–1675. [CrossRef]
22. Oh, K.S.; Chang, Y.W. Macro-segregation behavior in continuously cast high carbon steel blooms and billets at the final stage of solidification in combination stirring. *ISIJ Int.* **1995**, *35*, 866–875. [CrossRef]
23. Xiao, C.; Zhang, J.-M.; Luo, Y.-Z.; Wei, X.-D.; Wu, L.; Wang, S.-X. Control of macrosegregation behavior by applying final electromagnetic stirring for continuously cast high carbon steel billet. *J. Iron Steel Res. Int.* **2013**, *20*, 13–20. [CrossRef]
24. Zhang, Y.Y.; Yu, L.H.; Fu, T.; Wang, J.; Shen, Q.F.; Cui, K.K. Microstructure evolution and growth mechanism of Si-$MoSi_2$ composite coatings on TZM (Mo-0.5Ti-0.1Zr-0.02 C) alloy. *J. Alloys Compd.* **2022**, *894*, 162403. [CrossRef]
25. Zhang, Y.; Fu, T.; Cui, K.; Shen, F.; Wang, J.; Yu, L.; Mao, H. Evolution of surface morphology, roughness and texture of tungsten disilicide coatings on tungsten substrate. *Vacuum* **2021**, *191*, 110297. [CrossRef]
26. Zhang, Y.Y.; Cui, K.K.; Fu, T.; Wang, J.; Shen, F.Q.; Zhang, X.; Yu, L.H. Formation of $MoSi_2$ and Si/$MoSi_2$ coatings on TZM (Mo–0.5Ti–0.1Zr–0.02C) alloy by hot dip silicon-plating method. *Ceram. Int.* **2021**, *47*, 23053–23065. [CrossRef]
27. Rauter, W.; Reiter, J.; Srienc, K.; Brandl, W.; Erker, M.; Huemer, K.; Mair, A. Soft reduction at a round bloom caster: Implementation and results. *BHM Berg-Und Hüttenmänn. Mon.* **2014**, *159*, 454–460. [CrossRef]
28. Ma, H.; Zhang, J.; Cheng, R.; Wang, S. Numerical simulation study on quality control of the center macroscopic segregation in the continuous casting slab. *Trans. Indian Inst. Met.* **2019**, *72*, 825–835. [CrossRef]
29. Han, T.; Cheng, C.G.; Mei, J.X.; Zhu, J.F.; Jin, Y. Optimization of soft reduction process for continuous thick slab casting. *Adv. Mater. Res.* **2014**, *881-883*, 1558–1561. [CrossRef]
30. Tsuchida, Y.; Nakada, M.; Sugawara, I.; Miyahara, S.; Murakami, K.; Tokushige, S. Behavior of semi-macroscopic segregation in continuously cast slabs and technique for reducing the segregation. *Trans. Iron Steel Inst. Jpn.* **1984**, *24*, 899–906. [CrossRef]

31. Haida, O.; Kitaoka, H.; Habu, Y.; Kakihara, S.; Bada, H.; Shiraishi, S. Macro- and semi-macroscopic features of the centerline segregation in CC slabs and their effect on product quality. *Trans. Iron Steel Inst. Jpn.* **1984**, *24*, 891–898. [CrossRef]
32. Rosenthal, D.; Krämer, S.; Klein, C.; Geerkens, C.; Mueller, J. 20 years of CSP: Success story of an extraordinary technology. *Müller Stahl Und Eisen* **2009**, *129*, 73–86.
33. Hoen, K.; Klein, C.; Krämer, S.; Chung, J.S. Recent Development of Thin Slab Casting and Rolling Technology in a Challenging Market. In Proceedings of the 10th Int. Rolling Conf. and the 7th European Rolling Conference, Congress Graz, Graz, Austria, 6–9 June 2016; p. 1217.
34. Janssen, H.; Sowka, E. Seven years of progress in the casting-rolling plant at Thyssen Krupp Steel. *Stahl Und Eisen* **2007**, *127*, 27–33.
35. Klinkenberg, C.; Kintscher, B.; Hoen, K.; Reifferscheid, M. More than 25 Years of experience in thin slab casting and rolling current state of the art and future developments. *Steel Res. Int.* **2017**, *88*, 1700272. [CrossRef]
36. Fu, T.; Cui, K.; Zhang, Y.; Wang, J.; Shen, F.; Yu, L.; Qie, J.; Zhang, X. Oxidation protection of tungsten alloys for nuclear fusion applications: A comprehensive review. *J. Alloys Compd.* **2021**, *884*, 161057. [CrossRef]
37. Kaspar, R. Microstructural aspects and optimization of thin slab direct rolling of steels. *Steel Res. Int.* **2003**, *74*, 318–326. [CrossRef]
38. Choudhary, S.K.; Ganguly, S. Morphology and segregation in continuously cast high carbon steel billets. *ISIJ Int.* **2007**, *47*, 1759–1766. [CrossRef]
39. Saeki, T.; Imura, H.; Oonishi, Y.; Niimi, H.; Miwa, E.; Yoshida, T.; Igari, S.; Kitamine, S. Effect of bulging and solidification structure on segregation in continuously cast slab. *Trans. Iron Steel Inst. Jpn.* **1984**, *24*, 907–916. [CrossRef]
40. Pikkarainen, T.; Vuorenmaa, V.; Rentola, I.; Leinonen, M.; Porter, D. Effect of superheat on macrostructure and mac-ro-segregation in continuous cast low-alloy steel slabs. *Iop Conf.* **2016**, *117*, 012064.
41. Gadellaa, R.F.; Kreijger, P.J.; Cornelissen, M.C.M.; Donnay, B.; Herman, J.C.; Leroy, V. Metallurgical aspects of thin slab casting and rolling of low carbon steels. In Proceedings of the 2nd European Conference Continuous Casting (METEC 94), Dusseldorf, Germany, 20–22 June 1994; Volume 1, pp. 382–389.
42. Clyne, T.W.; Kurz, W. Solute redistribution during solidification with rapid solid state diffusion. *Met. Mater. Trans. A* **1981**, *12*, 965–971. [CrossRef]
43. Meng, Y.; Thomas, B. Heat-transfer and solidification model of continuous slab casting: CON1D. *Met. Mater. Trans. A* **2003**, *34*, 685–705. [CrossRef]
44. Ueshima, Y.; Mizoguchi, S.; Matsumiya, T.; Kajioka, H. Analysis of solute distribution in dendrites of carbon steel with δ/γ transformation during solidification. *Met. Mater. Trans. A* **1986**, *17*, 845–859. [CrossRef]
45. Kajatani, T.; Drezet, J.-M.; Rappaz, M. Numerical simulation of deformation-induced segregation in continuous casting of steel. *Met. Mater. Trans. A* **2001**, *32*, 1479–1491. [CrossRef]
46. Miyazawa, K.; Schwerdtfeger, K. Macrosegregation in continuously cast steel slabs: Preliminary theoretical investigation on the effect of steady state bulging. *Archiv Eisenhüttenwes.* **1981**, *52*, 415–422. [CrossRef]
47. Chakraborty, S.; Dutta, P. Effects of dendritic arm coarsening on macroscopic modelling of solidification of binary alloys. *Mater. Sci. Technol.* **2001**, *17*, 1531–1538. [CrossRef]
48. Poirier, D.R. Permeability for flow of interdendritic liquid in columnar-dendritic alloys. *Met. Mater. Trans. A* **1987**, *18*, 245–255. [CrossRef]
49. Yoo, H.; Viskanta, R. Effect of anisotropic permeability on the transport process during solidification of a binary mixture. *Int. J. Heat Mass Transf.* **1992**, *35*, 2335–2346. [CrossRef]
50. Ahmad, N.; Rappaz, J.; Desbiolles, J.-L.; Jalanti, T.; Rappaz, M.; Combeau, H.; Lesoult, G.; Stomp, C. Numerical simulation of macrosegregation: A comparison between finite volume method and finite element method predictions and a confrontation with experiments. *Met. Mater. Trans. A* **1998**, *29*, 617–630. [CrossRef]
51. Yamanaka, A.; Nakajima, K.; Yasumoto, K.; Kawashima, H.; Nakai, K. New evaluation of critical strain for internal crack formation in continuous casting. *Rev. Métall.* **1992**, *89*, 627–634. [CrossRef]
52. Cornelissen, M.C.M. Mathematical model for solidification of multi component alloys. *Ironmak. Steelmak.* **1986**, *13*, 204–212.